Chapter 16
Analysis of Dislocations in Quasicrystals Composed of Self-assembled Nanoparticles

Liron Korkidi, Kobi Barkan, and Ron Lifshitz

Abstract We analyze transmission electron microscopy (TEM) images of self-assembled quasicrystals composed of binary systems of nanoparticles. We use an automated procedure that identifies the positions of dislocations and determines their topological character. To achieve this, we decompose the quasicrystal into its individual density modes, or Fourier components, and identify their topological winding numbers for every dislocation. This procedure associates a Burgers function with each dislocation, from which we extract the components of the Burgers vector after choosing a basis. The Burgers vectors that we see in the experimental images are all of lowest order, containing only 0s and 1s as their components. We argue that the density of the different types of Burgers vectors depends on their energetic cost.

16.1 Dislocations in Self-assembled Soft-Matter Quasicrystals

Self-assembled soft-matter quasicrystals have been observed in recent years in a wide variety of different systems, in all cases but one with dodecagonal (12-fold) point-group symmetry. First discovered by Zeng et al. [21] in liquid crystals made of micelle-forming dendrimers, self-assembled soft-matter quasicrystals have since appeared in other systems such as ABC-star polymers [9], in binary systems of nanoparticles [16], in block co-polymer micelles [6], and in mesoporous silica [20]. These newly-realized systems not only provide exciting platforms for the fundamental study of the physics of quasicrystals [2], they also hold the promise for new and exciting applications, especially in the field of photonics. An overview of soft matter quasicrystals, including many references relevant to these systems, is given by Lifshitz and Diamant [14] as well as by Ungar et al. [17, 18] and Dotera [4, 5].

Here we concentrate on the systems of nanoparticles studied by Talpin et al. [16], consisting typically of two types of particles, such as PbS, Au, Fe_2O_3, and Pd,

L. Korkidi · K. Barkan · R. Lifshitz (✉)

Raymond and Beverly Sackler School of Physics and Astronomy, Tel Aviv University, Tel Aviv 69978, Israel

e-mail: ronlif@tau.ac.il

with different diameters. These binary systems of particles, when placed in a solution, self-assemble into structures with long-range order, including 12-fold symmetric quasicrystals. The dimensions of the particles—typically a few nanometers in diameter—are such that they can be imaged directly using a transmission electron microscope (TEM). This allows one to study effects that are inaccessible with atomic-scale quasicrystals. Here we present a quantitative analysis of the dislocations that are naturally formed in these quasicrystals as they self-assemble.

In periodic crystals in d-dimensions, one can usually identify the position of a dislocation rather easily by the termination of a plane of atoms in three dimensions, or a line of atoms in two dimensions. One then chooses a basis for the periodic lattice; encircles each dislocation with a Burgers loop, or a Burgers circuit, of basis vectors; and counts the accumulated difference between the number of steps taken forward and backward in the direction of each of the d basis vectors. The d integers thus obtained define the Burgers vector which encodes the topological character of the dislocation. A similar real-space procedure can be used on a quasiperiodic crystal by overlaying it with a quasiperiodic tiling of rank $D > d$ (for a definition, see below), yielding a D-component Burgers vector [19]. A tiling-based analysis [10] of binary systems of nanoparticles was indeed recently carried out by Bodnarchuk et al. [3]. Here we propose an alternative approach for analyzing dislocations in Fourier space that we believe is useful when dealing with aperiodic crystals.

16.2 Density Modes, Winding Numbers, and the Burgers Function

Let us describe the density of nanoparticles in a self-assembled crystal by a function $\rho(\mathbf{r})$. The Fourier expansion of such a function is given by

$$\rho(\mathbf{r}) = \sum_{\mathbf{k} \in L} \rho(\mathbf{k}) e^{i\mathbf{k}\cdot\mathbf{r}}, \tag{16.1}$$

where the (reciprocal) lattice L is a finitely generated $\mathbb{Z}$-module, which means that it can be expressed as the set of all integral linear combinations of a finite number D of d-dimensional wave vectors, $\mathbf{b}^{(1)}, \ldots, \mathbf{b}^{(D)}$. In the special case where the smallest possible D, called the *rank* of the crystal, is equal to the physical dimension d, the crystal is periodic. More generally, for quasiperiodic crystals $D \geq d$, and we refer to all quasiperiodic crystals that are not periodic as *quasicrystals* [11, 12].

As explained elsewhere [13], the topological nature of a dislocation is related to the fact that it cannot be made to disappear by local structural changes. For this to be the case, as one follows a loop around the position of a dislocation and returns to the point of origin, one sees a crystal that is everywhere only-slightly distorted from the perfectly ordered state, except near the core of the dislocation. In particular, the complex amplitudes $\rho(\mathbf{k})$ of the density modes maintain their magnitudes along the loop, each accumulating at most a phase, which upon return to the point of origin must be an integer multiple of 2π. The collection of all such integers, or so-called

winding numbers, for a given dislocation defines a linear function $\mathcal{N}_\mathcal{B}(\mathbf{k})$ from the lattice L to the set of integers $\mathbb{Z}$, which we call the *Burgers function*.

The Burgers function of a given dislocation associates a particular winding number $\mathcal{N}_\mathcal{B}(\mathbf{k})$ with every wave vector $\mathbf{k} \in L$. Because this function is linear, after choosing a basis $\{\mathbf{b}^{(i)}\}$ for the lattice, it is uniquely specified by a set of only D integers $n_i \equiv \mathcal{N}_\mathcal{B}(\mathbf{b}^{(i)})$, forming the *Burgers vector* $(n_1, \ldots, n_D)$. Thus,

$$\forall \mathbf{k} = \sum_{i=1}^{D} a_i \mathbf{b}^{(i)} \in L: \quad \mathcal{N}_\mathcal{B}(\mathbf{k}) = \sum_{i=1}^{D} a_i \mathcal{N}_\mathcal{B}(\mathbf{b}^{(i)}) = \sum_{i=1}^{D} a_i n_i, \quad (16.2)$$

where $a_i \in \mathbb{Z}$. This implies that in order to fully characterize a dislocation in an experimental image it suffices to isolate the D density modes associated with a chosen basis, and obtain their corresponding winding numbers. This is the basis of the approach presented below for analyzing dislocations (for more detail, see [1, 7, 8]).

16.3 Analysis of the Dislocations in a Quasicrystal of Nanoparticles

We begin with a high-resolution TEM image of one of the dodecagonal quasicrystals grown by Talapin [15], a section of which is shown in Fig. 16.1(a). This particular quasicrystal is self-assembled from 11.2 nm PbS and 5.2 nm Au nanoparticles, and contains a distribution of dislocations that are formed naturally during the self assembly. We Fourier transform the TEM image, to obtain the diffraction image shown in Fig. 16.1(b), and then choose four of the Bragg peaks in the 12-fold ring containing the strongest reflections as a basis $\mathbf{b}^{(1)}, \ldots, \mathbf{b}^{(4)}$ for the reciprocal lattice. These are labeled in the schematic representation of the lattice in Fig. 16.2.

For each of the four pairs of Bragg peaks, associated with the chosen basis vectors and their negatives, we then carry out the following procedure:

1. We filter out small regions around the two opposite Bragg peaks, as indicated by a pair of red circles in Fig. 16.1(b) for the case of the density mode associated with the wave vectors $\pm \mathbf{b}^{(1)}$.
2. We invert the Fourier transform in the filtered regions resulting in a real-space image of a single density mode. Dislocations appear as discontinuities in the stripes. We use a routine that identifies all the discontinuities and marks their positions, as shown in Fig. 16.1(c) for this density mode.
3. For each dislocation, a second routine then extracts the ith component $n_i = \mathcal{N}_\mathcal{B}(\mathbf{b}^{(i)})$ of the Burgers vector. This is done by enclosing a counter-clockwise loop around its position and calculating the accumulated phase in units of 2π. Practically what we do is count the number of stripes crossed moving in the direction of the wave vector $\mathbf{b}^{(i)}$ on one side of the dislocation, and subtract the number of stripes crossed moving against the direction of $\mathbf{b}^{(i)}$ while returning on the other side, as demonstrated in Fig. 16.3.
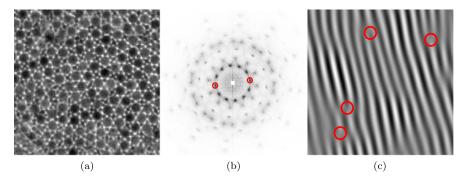
(a)   (b)   (c)

Fig. 16.1 (**a**) A section of a TEM image of a dodecagonal quasicrystal, self-assembled from 11.2 nm PbS and 5.2 nm Au showing several dislocations (courtesy of Dmitri Talapin 2012). (**b**) Fourier transform of the TEM image in (**a**), with the central peak blocked. A pair of Bragg peaks, associated with one of the basis vectors and its negative, is marked in *red*. (**c**) The corresponding section of the inverse Fourier transform of the Bragg peaks marked in (**b**) with *red circles* marking the positions of four dislocations
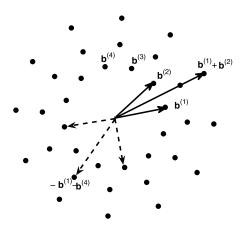

Fig. 16.2 Schematic representation of the three strongest rings in the Fourier transform of our dodecagonal quasicrystal. The inner ring is the strongest, containing the four basis vectors $\mathbf{b}^{(1)}, \ldots, \mathbf{b}^{(4)}$. The second strongest ring is the outer one, obtained from all the sums of two adjacent vectors in the inner ring, as indicated by *solid arrows*. The third strongest ring lies in between, obtained from all sums of vector pairs in the inner ring that are separated by 90 degrees, as indicated by *dashed arrows*

Finally, we verify the correctness of the calculation by extracting the values $\mathcal{N}_{\mathcal{B}}(\mathbf{k})$ for additional wave vectors $\mathbf{k}$ and checking that they satisfy the linearity requirement given by Eq. (16.2).
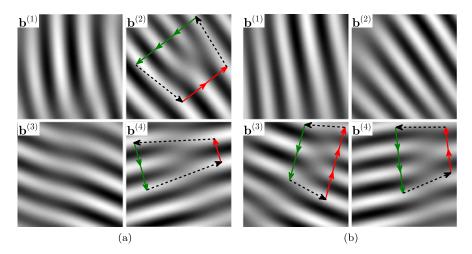
Fig. 16.3 Two typical examples for the dislocations found using our procedure. In each counter–clockwise loop, the winding number n_i is given by the number of *red arrows*, counting stripes crossed in the positive direction of $\mathbf{b}^{(i)}$, minus the number of *green arrows*, counting stripes in the negative direction. (**a**) A *single-subset* dislocation with Burgers vector $(0, -1, 0, -1)$ and (**b**) a *dual-subset* dislocation with Burgers vector $(0, 0, 1, -1)$ (see text for definitions)

16.4 Results and Discussion

We typically find a density of a few dozen dislocations per μm^2 in the nanoparticle quasicrystals of [15]. All of these dislocations are of lowest order in the sense that $n_i = 0$, 1, or -1. To understand the topological nature of these dislocations, it is useful to classify them by dividing the four basis vectors into two hexagonal subsets, $\{\mathbf{b}^{(1)}, \mathbf{b}^{(3)}\}$ and $\{\mathbf{b}^{(2)}, \mathbf{b}^{(4)}\}$ (see Fig. 16.2). By doing so, we find that the density of dislocations with non-zero components in only one of the subsets, which we call *single-subset* dislocations, is five times larger than that of dislocations with non-zero components in both subsets, which we call *dual-subset* dislocations. Examples of the two types of dislocations are shown in Fig. 16.3.

To try and explain these observations, consider the free energy of the self-assembled crystal as an expansion in products of density mode amplitudes $\rho(\mathbf{k})$ (see [13]),

$$\mathcal{F}\{\rho\} = \sum_{n=2}^{\infty} \sum_{\mathbf{k}_1 \ldots \mathbf{k}_n} A(\mathbf{k}_1, \ldots, \mathbf{k}_n) \rho(\mathbf{k}_1) \cdots \rho(\mathbf{k}_n), \tag{16.3}$$

where one can show that $A(\mathbf{k}_1, \ldots, \mathbf{k}_n) = 0$ unless $\mathbf{k}_1 + \cdots + \mathbf{k}_n = 0$. We argue that products in the sum (16.3) that contain high-intensity modes with large winding numbers have a greater contribution to increasing the free energy away from its minimum value in the perfect crystal. Accordingly, high-intensity modes tend to exhibit smaller winding numbers. Indeed, we find that all the winding numbers associated with the two brightest rings (see Fig. 16.1(b) and Fig. 16.2) are either 0 or

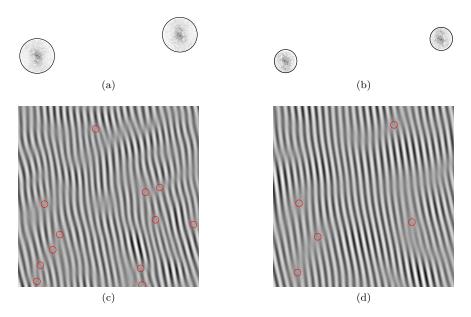(a)　　　　　　　　　　　　　　　　　　　　　　　　　　　　(b)

(c)　　　　　　　　　　　　　　　　　　　　　　　　　　　　(d)

Fig. 16.4 Inverse Fourier transform of a pair of Bragg peaks using filters of different size. For a circular filter with a radius of 25 pixels, used in (**a**), we find 12 dislocations, marked with red circles in (**c**). As we decrease the filter radius to 15 pixels, in (**b**), we find only 5 dislocations in the inverse Fourier transform in (**d**)

± 1, whereas it is only on the 3rd ring that we begin to see winding numbers that are either 0, ± 1, or ± 2. Moreover, owing to the linearity of the Burgers function, the fact that the winding numbers on the second brightest ring are at most of magnitude 1 prevents two adjacent peaks from the different subsets in the first ring from having non-zero winding numbers of the same sign. Because the ring of Bragg peaks, obtained by adding pairs of wave vectors separated by 60 degrees, is extremely weak (see Fig. 16.1(b)), there is no such constraint on the winding numbers belonging to the same subset of basis vectors. The fact that this constraint applies only to dual-subset dislocations reduces their possible combinations and overall relative density.

A word of caution is in order regarding our approach for analyzing dislocations. Because the density of the dislocations is relatively high, the Bragg peaks are not point-like but are rather spread as can be seen in Fig. 16.1(b). This means that some of the information about the dislocations may lie between Bragg peaks and may be lost if the filters are too small. Therefore, our approach is sensitive to the shape and size of the filter that we use around each Bragg peak. As we increase the filter size we obtain more information and potentially find more dislocations, as demonstrated in Fig. 16.4. We thus try to optimize the filter by gradually enlarging its size until the number of dislocations stops increasing substantially.

Our approach for analyzing dislocations should be easily adapted to other systems even when the density of the dislocations is quite large, as one may expect for soft matter systems. Moreover, for dynamical systems that can be imaged in real

time one can use our automated method to follow and quantitatively analyze the dynamics of the dislocations.

References

1. Barak, G, Lifshitz, R (2006) Dislocation dynamics in a dodecagonal quasiperiodic structure. Philos Mag 86:1059. doi:10.1080/14786430500256383
2. Barkan, K, Diamant, H, Lifshitz, R (2011) Stability of quasicrystals composed of soft isotropic particles. Phys Rev B 83:172201. doi:10.1103/PhysRevB.83.172201
3. Bodnarchuk, MI, Shevchenko, EV, Talapin, DV (2011) Structural defects in periodic and quasicrystalline binary nanocrystal superlattices. J Am Chem Soc 133:20837. doi:10.1021/ja207154v
4. Dotera, T (2011) Quasicrystals in soft matter. Isr J Chem 51:1197–1205. doi:10.1002/ijch.201100146
5. Dotera, T (2012) Toward the discovery of new soft quasicrystals: from a numerical study viewpoint. J Polym Sci, Polym Phys Ed 50:155–167. doi:10.1002/polb.22395
6. Fischer, S, Exner, A, Zielske, K, Perlich, J, Deloudi, S, Steurer, W, Lindner, P, Förster, S (2011) Colloidal quasicrystals with 12-fold and 18-fold diffraction symmetry. Proc Natl Acad Sci USA 108:1810–1814. doi:10.1073/pnas.1008695108
7. Freedman, B, Bartal, G, Segev, M, Lifshitz, R, Christodoulides, DN, Fleischer, JW (2006) Wave and defect dynamics in nonlinear photonic quasicrystals. Nature 440:1166–1169. doi:10.1038/nature04722
8. Freedman, B, Lifshitz, R, Fleischer, JW, Segev, M (2007) Phason dynamics in nonlinear photonic quasicrystals. Nat Mater 6:776–781. doi:10.1038/nmat1981
9. Hayashida, K, Dotera, T, Takano, A, Matsushita, Y (2007) Polymeric quasicrystal: mesoscopic quasicrystalline tiling in ABC star polymers. Phys Rev Lett 98:195502. doi:10.1103/PhysRevLett.98.195502
10. Leung PW, Henley CL, Chester GV (1989) Dodecagonal order in a two-dimensional Lennard–Jones system. Phys Rev B 39:446–458. doi:10.1103/PhysRevB.39.446
11. Lifshitz, R (2003) Quasicrystals: a matter of definition. Found Phys 33:1703–1711
12. Lifshitz, R (2007) What is a crystal? Z Kristallogr 222:313–317. doi:10.1524/zkri.2007.222.6.313
13. Lifshitz, R (2011) Symmetry breaking and order in the age of quasicrystals. Isr J Chem 51:1156. doi:10.1002/ijch.201100156
14. Lifshitz, R, Diamant, H (2007) Soft quasicrystals—why are they stable? Philos Mag 87:3021. doi:10.1080/14786430701358673
15. Talapin, DV (2012) Private communication
16. Talapin, DV, Shevchenko, EV, Bodnarchuk, MI, Ye, X, Chen, J, Murray, CB (2009) Quasicrystalline order in self-assembled binary nanoparticle superlattices. Nature 461:964. doi:10.1038/nature08439
17. Ungar, G, Zeng, X (2005) Frank–Kasper, quasicrystalline and related phases in liquid crystals. Soft Matter 1:95–106. doi:10.1039/B502443A
18. Ungar, G, Percec, V, Zeng, X, Leowanawat, P (2011) Liquid quasicrystals. Isr J Chem 51:1206–1215. doi:10.1002/ijch.201100151

19. Wollgarten M, Franz V, Feuerbacher M, Urban K (2002) In: Suck J-B, Schreiber M, Hussler P (eds) Quasicrystals: an introduction to structure, physical properties, and applications. Springer, Berlin, Chap. 13

20. Xiao, C, Fujita, N, Miyasaka, K, Sakamoto, Y, Terasaki, O (2012) Dodecagonal tiling in mesoporous silica. Nature 487:349. doi:10.1038/nature11230

21. Zeng, X, Ungar, G, Liu, Y, Percec, V, Dulcey, AE, Hobbs, JK (2004) Supramolecular dendritic liquid quasicrystals. Nature 428:157–160. doi:10.1038/nature02368